SCIENCE CHINA
Technological Sciences

• Article •

May 2017 Vol.60 No.5: 713–725
doi: 10.1007/s11431-016-0452-8

Modeling and optimal energy management of a power split hybrid electric vehicle

SHI DeHua[1,2], WANG ShaoHua[1], Pierluigi Pisu[2], CHEN Long[1*], WANG RuoChen[1*] & WANG RenGuang[3]

[1] *School of Automotive and Traffic Engineering, Jiangsu University, Zhenjiang 212013, China;*
[2] *Clemson University International Center for Automotive Research, Greenville, SC 29607, USA;*
[3] *China Automotive Technology and Research Center, Tianjin 300300, China*

Received June 8, 2016; accepted September 29, 2016; published online December 6, 2016

With the combination of engine and two electric machines, the power split device allows higher efficiency of the engine. The operation modes of a power split HEV are analyzed, and the system dynamic model is established for HEV forward simulation and controller design. Considering the fact that the operation modes of the HEV are event-driven and the system dynamics is continuous time-driven for each mode, the structure of the controller is built and described with the hybrid automaton control theory. In this control structure, the mode selection process is depicted by the finite state machine (FSM). The multi-mode switch controller is designed to realize power distribution. Furthermore, the vehicle mode operations are optimized, and the nonlinear model predictive control (NMPC) strategy is applied by implementing dynamic programming (DP) in the finite prediction horizon. Comparative simulation results demonstrate that the hybrid control structure is effective and feasible for HEV energy management design. The NMPC optimal strategy is superior in improving fuel economy.

hybrid electric vehicle, power split, energy management, model predictive control, hybrid system

Citation: Shi D H, Wang S H, Pierluigi P, et al. Modeling and optimal energy management of a power split hybrid electric vehicle. Sci China Tech Sci, 2017, 60: 713–725, doi: 10.1007/s11431-016-0452-8

1 Introduction

Having extra power source and electrical machines, hybrid electric vehicles (HEVs) allow downsizing and better operation points of the engine, as well as energy recuperating during braking, resulting in the reduction of fuel consumption and exhaust emissions [1]. Generally, the configurations of HEV powertrain can be classified into three types: parallel, series and series-parallel. Among different architectures, the series-parallel HEVs, or power split HEVs, are superior in enabling the engine to operate in high efficiency regions because the engine speed is decoupled from the vehicle speed by power split devices (planetary gear set) [2]. The power split devices can also act as electric continuous variable transmission (ECVT) [3]. Typical examples of power split HEVs include Toyota Prius hybrid synergy drive systems (THS), GM-Allison designs, and so on [4,5].

With the introduction of mechanical devices, such as clutches and/or brakes, into the planetary gear sets, the power split HEVs have more operation modes [6]. When an extra clutch is added to the Prius transmission, the fuel economy of this new power split HEV is improved significantly in urban driving conditions [7]. A novel power split configuration was proposed in ref. [8], which had the same topology as that of a conventional four-speed automatic transmission. The power split HEV could realize as many as

*Corresponding authors (email: chenlong@ujs.edu.cn; wrc@ujs.edu.cn)

nine operation modes and, in comparison with a benchmark vehicle, result in 5.62% fuel reduction. In ref. [9], the performance of the power split configurations with double planetary gear sets and triple planetary gear sets were compared in qualitative and quantitative ways.

To fully exploit the advantages of power split configurations, energy management strategy (EMS) should be stressed. Without appropriate EMS, even the best architecture will operate poorly [10]. HEV control strategies can be mainly classified as rule-based control strategies and optimization-based strategies [11]. Rule-based strategy, usually derived from engineering expertise and heuristics, can ensure the real-time energy flow between different sources. Rule-based strategy decides the control schemes of each component according to the current powertrain state when a priori driving cycle is unknown. Depending on the engaging/disengaging states of the clutches and/or brakes, there are various operation modes for power split HEVs with clutches and/or brakes. Different operation modes usually correspond to different models of power split configuration. Due to the fact that the model-based approach is based on a simple and adequately accurate control-oriented model, it is hard to develop model-based optimal control approach for such power split HEVs [10]. Consequently, rule-based strategy is widely used in the power split powertrain with clutches and/or brakes for real-time control [8]. Fuzzy control is another kind of rule-based methods used in HEV energy management [12]. Switching thresholds and fuzzy control rules can be optimized to better distribute power flow between different sources [13,14]. Dynamic programming (DP), the global optimization method, is adopted to find a global optimal solution based on the Bellman principle. However, DP is highly a priori driving cycle dependent and computationally demanding, thus simplified HEV model is often used to ease the computational burden. The global optimal solution of DP for a certain driving cycle is derived off-line and acts as a benchmark for other optimal control techniques. The off-line optimization method, on the basis of back propagation through time (BPTT) like algorithm, was implemented to find the optimal control trajectories for a power split HEV with dual-planetary gear sets [15]. To meet the real-time requirements, the instantaneous optimization based on Pontryagin's minimum principle (PMP) can be formulated and conducted [16]. Similar to the optimal control based on PMP, equivalent minimization fuel consumption (ECMS) control has been developed to optimize the power flow [17,18] by equating the usage of electrical energy to fuel consumption. Nevertheless, the optimal solutions of both PMP real-time optimal control and ECMS are sensitive to the driving cycles. Initial control parameters should be regulated for certain driving cycle. The fuel economy may deteriorate when the predefined control parameters are applied under other driving conditions. Model predictive control (MPC) is used to formulate the optimal energy management problem of HEV within a receding finite horizon as a compromise optimal control problem between global optimization and instantaneous optimization. Borhan et al. [19] considered the energy management problem of the Toyota Prius as a constrained and nonlinear optimal control problem, and MPC was adopted to obtain the optimal power split. In ref. [20], the engine transient characteristics were incorporated in the MPC torque split strategy, and the proposed strategy demonstrated superior fuel efficiency while maintaining driving performance.

In this study, the power split powertrain developed by China Automotive Technology & Research Center is analyzed and modeled [21]. The topology scheme of the powertrain is shown in Figure 1. The engine is connected to the carrier gear C1 of the first planetary gear set via a buffer and locking mechanism. Two electric machines, MG1 and MG2, are connected to the first sun gear S1 and the second sun gear S2, respectively. The buffer and locking mechanism can allow easier control of C1 and alleviate the rotational shocks from the engine. In most situations, MG1 acts as a generator to charge the battery and as a speeder to regulate the engine speed when the locking mechanism is disengaged. When the locking mechanism is locked, compound driving with the two electric machines is realized, resulting in the improvement of dynamic performance in pure electric mode.

The proposed HEV can operate in different modes by controlling the on/off states of the engine, motors and the buffer and locking mechanism. In each operation mode, the system state variables, such as the battery SOC and motor speed, evolve according to the dynamic equations constrained by corresponding physical properties. The system shows continuous dynamics. However, the mode switches are caused by a series of discrete events according to the decision information. The HEV operation process shows typical hybrid dynamic characteristics [22,23]. The control scheme of the system can be designed with the hybrid system theory.

Based on hybrid automaton control theory, this paper ex-

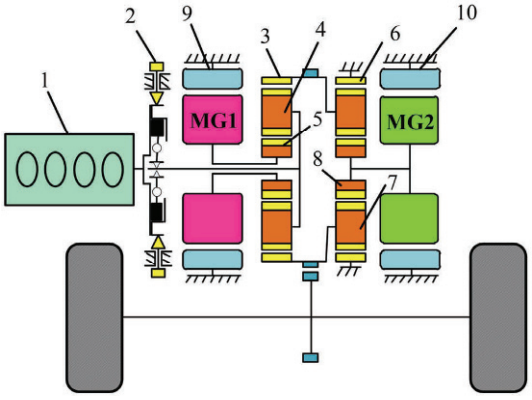

Figure 1 (Color online) Topology of power split configuration, 1-engine, 2-locking mechanism, 3-ring gear R1, 4-carrier gear C1, 5-sun gear S1, 6-ring gear R2, 7-carrier gear C2, 8-sun gear S2, 9-electric machine MG1, 10-electric machine MG2.

plores the modeling and optimal control design of a power split HEV. Specifically, the rest of the paper is organized as follows. Section 2 establishes the dynamic model of the system. In Section 3, the HEV controller is constructed based on hybrid automaton control theory. The application of NMPC is investigated in Section 4, followed by comparative simulations and analyses in Section 5. In the end, conclusions are drawn in Section 6.

2 Modeling of the plant

The forward simulation model is established for the controller design and fuel economy estimation. The static models of engine, motor, generator and battery are used. Meanwhile, the damping and compliance are ignored. These simplifications are feasible to evaluate the system performance in terms of fuel economy. The top level simulation model can be inspired by ref. [8].

2.1 Operation modes

Generally, there are three states (modes) of the vehicle, i.e., driving, standstill and braking (denoted by m_A, m_B and m_C, respectively), which can be decided by the driver torque requirements T_{req}. Each of the three states includes several final states for the control decision, as detailed in Table 1. Table 1 also depicts the states of the locking mechanism, engine, motor and generator in each mode. When the power split HEV is in the modes of MG2 only driving, regenerative braking and mechanical braking, locking mechanism can be controlled to be either engaged or disengaged. The engaged and disengaged states of the locking mechanism correspond to the off and on states of the generator, respectively. In this research, the locking mechanism is controlled to be disengaged for the synthesis of the optimal EMS. Such control is reasonable because the power used to regulate the engine speed and consumed by the generator is very small. In this way, the locking mechanism is engaged only when HEV operates in the mode of compound pure electric driving (MG1 and MG2 compound driving). The powertrain model can be synthesized. Besides, since the compound pure electric driving mode only operates under high-load, engaging the locking mechanism just in this mode can reduce the operation frequency of the locking mechanism greatly. The life cycle of the locking mechanism is extended.

2.2 Modeling

Based on lever analogy [8], torque relations of power split architecture are obtained, as shown in Figure 2. The shafts of the HEV powertrain are all assumed to be rigid, and inertias of the pinions in the carrier gears are ignored. In the figure, ω_{S1}, ω_{C1} and ω_{R1} denote the rotational speed of S1, C1 and R1, respectively. I_{S1}, I_{C1} and I_{R1} are lumped inertias corresponding to each gear. These definitions are also applicable for PG2. The ring gear R1 of PG1 is connected to the carrier gear C2 of PG2. Hence, an inner torque T_{in} exists between R1 and C2. K_1 is the characteristic parameter of PG1, and K_2 the characteristic parameter of PG2. They denote the ratio of tooth number between the ring gear and sun gear. T_{R2} is the external torque from the shell, which fixes R2. Consequently, the rotational speed of R2 is zero. T_{S1} is the external torque applied to S1 from MG1, while T_{C1}, T_{C2} and T_{S2} are external torque applied to C1, C2 and S2, respectively.

According to the lever analogy, both PG1 and PG2 have one rotational degree of freedom (DoF) and one translational DoF. For PG1, the dynamic equations are

$$T_{C1}+T_{S1}-T_{in}-I_{R1}\dot{\omega}_{R1}-I_{C1}\dot{\omega}_{C1}-I_{S1}\dot{\omega}_{S1}=0, \tag{1}$$

$$T_{S1}\left(1+K_1\right)+T_{C1}-I_{S1}\dot{\omega}_{S1}\left(1+K_1\right)-I_{C1}\dot{\omega}_{C1}=0, \tag{2}$$

where eqs. (1) and (2) denote the equilibrium equations of the translational DoF and rotational DoF, respectively. In the same way, the dynamic equations of PG2 can also be derived, as given by

$$T_{S2}-T_{C2}+T_{R2}+T_{in}-I_{R2}\dot{\omega}_{R2}-I_{C2}\dot{\omega}_{C2}-I_{S2}\dot{\omega}_{S2}=0, \tag{3}$$

$$T_{S2}K_2+I_{R2}\dot{\omega}_{R2}-I_{S2}\dot{\omega}_{S2}K_2-T_{R2}=0. \tag{4}$$

Table 1 Operation modes

Discrete state of HEV		Locking mechanism	Engine	Motor	Generator
Implicit state	Final state				
Driving (m_A)	MG2 only driving (m_{A1})	engaged/disengaged	off	on	off/on
	MG1 and MG2 compound driving (m_{A2})	engaged	off	on	on
	hybrid driving (m_{A3})	disengaged	on	on	on
	engine start (m_{A4}, m_{B1})	disengaged	on	on	on
		disengaged	on	off	on
Standstill (m_B)	Stop (m_{B2})	disengaged	off	off	off
	charging while standstill (m_{B3})	disengaged	on	on	off
Braking (m_C)	regenerative braking (m_{C1})	engaged/disengaged	off	on	off/on
	mechanical braking (m_{C2})	engaged/disengaged	off	off	off/on

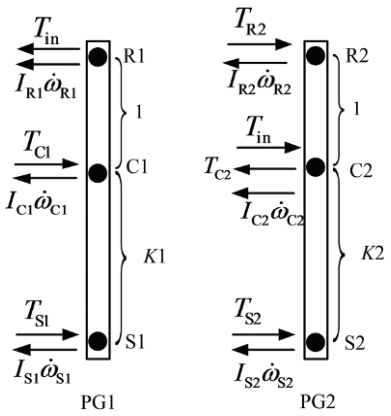

Figure 2 Torque analysis of power-split architecture.

The rotational speed of the planetary gears has the following relations:

$$(1+K_1)\omega_{C1}=\omega_{S1}+K_1\omega_{R1}, \tag{5}$$

$$(1+K_2)\omega_{C2}=\omega_{S2}+K_2\omega_{R2}. \tag{6}$$

Since the engine, MG1 and MG2 are directly connected to C1, S1 and S2, respectively, we have

$$\omega_G=\omega_{S1}, \tag{7}$$

$$\omega_M=\omega_{S2}, \tag{8}$$

$$\omega_E=\omega_{C1}, \tag{9}$$

where ω_E, ω_G, and ω_M are rotational speeds of the engine, MG1 and MG2, respectively. The rotational speed ω_{out} at the input side of the final drive is equal to the rotational speed of C2, and is decided by the vehicle velocity

$$\omega_{out}=\omega_{C2}=\frac{vi_d}{R_w}, \tag{10}$$

where v is the HEV velocity, R_w is the wheel radius, and i_d is the ratio of the final drive. External torque of S1 and S2 are related to MG1 and MG2. T_{S1} and T_{S2} are obtained by

$$T_{S1}=T_G-I_G\dot{\omega}_G, \tag{11}$$

$$T_{S2}=T_M-I_M\dot{\omega}_M, \tag{12}$$

where T_G and T_M are the torque of MG1 and MG2, respectively, while I_G and I_M denote the inertias. The external torque T_{C1} depends on the state of locking mechanism. When it is engaged, T_{C1} is provided by shell. When it is open, T_{C1} is

$$T_{C1}=T_E-I_E\dot{\omega}_E, \tag{13}$$

where T_E and I_E are the engine torque and inertia, respectively. T_{C2} is the load torque on C2, and is derived by

$$\begin{aligned}T_{out}=&T_{brk}/i_d+\left[Mg\left(f\cos\theta+\sin\theta\right)\right]R_w/i_d\\&+0.5\rho_{air}A_fC_d\left(\omega_{out}/i_d\right)^2R_w^3/i_d+I_{out}\dot{\omega}_{out},\end{aligned} \tag{14}$$

where M is the vehicle mass, g is the gravity acceleration, f is the coefficient of rolling resistance, θ is the road slope, ρ_{air} is the air density, C_d is the air drag coefficient and A_f is the vehicle frontal area. T_{brk} is the friction braking torque. Since the direction of T_{C2} is defined to be opposite to the driving torques in Figure 2, positive number of T_{brk} in eq. (14) is applied.

According to eqs. (1)–(14), the dynamic equations of HEV powertrain in different states of the locking mechanism are derived by eliminating the interaction force between R1 and C2.

When the locking mechanism is disengaged, the dynamic matrix equation is

$$\begin{aligned}\begin{bmatrix}\dot{\omega}_E\\ \dot{\omega}_{out}\end{bmatrix}=&\begin{bmatrix}I_{gt}\left(1+K_1\right)^2+I_{et} & -I_{gt}K_1\left(1+K_1\right)\\ I_{gt}\left(1+K_1\right)+I_{et} & -K_1I_{gt}+\left(1+K_2\right)^2I_{mt}+I_{outt}\end{bmatrix}^{-1}\\&\cdot\begin{bmatrix}\left(1+K_1\right)T_G+T_E\\ \left(1+K_2\right)T_M+T_E+T_G-T_{out}\end{bmatrix},\end{aligned} \tag{15}$$

when the locking mechanism is engaged, ω_{C1} equals zero, and the system equation is

$$\begin{aligned}\begin{bmatrix}\dot{\omega}_E\\ \dot{\omega}_{out}\end{bmatrix}=&\begin{bmatrix}0 & 0\\ 0 & \dfrac{1}{K_1^2I_{gt}+\left(1+K_2\right)^2I_{mt}+I_{outt}}\end{bmatrix}\\&\cdot\begin{bmatrix}0\\ \left(1+K_2\right)T_M-K_1T_G-T_{out}\end{bmatrix}.\end{aligned} \tag{16}$$

In eqs. (15) and (16), the lumped inertias is calculated as:

$$\begin{cases}I_{et}=I_E+I_{C1},\\ I_{gt}=I_G+I_{S1},\\ I_{mt}=I_M+I_{S2},\\ I_{outt}=I_{R1}+I_{C2}+I_{fd}+\left(MR_w^2+4I_w\right)/i_d^2,\end{cases} \tag{17}$$

where I_{fd} is the inertia of the final drive, I_w is the inertia of each wheel.

The behavior of the battery is characterized by the battery state of charge (SOC) dynamics. The SOC is also a main state variable when designing HEV optimal control strategy. The battery dynamics is modeled as:

$$\dot{\mathrm{SOC}}=-\frac{V_{oc}-\sqrt{V_{oc}^2-4P_{bat}R_{int}}}{2Q_{bat}R_{int}}, \tag{18}$$

where V_{oc} is the open-circuit voltage of the battery, Q_{bat} is the battery capacity, and R_{int} is internal resistance. P_{bat} is the battery power, which relies on the power of the motor and generator

$$P_{\text{bat}} = T_{\text{M}}\omega_{\text{M}}\eta_{\text{M}}^{\lambda} + T_{\text{G}}\omega_{\text{G}}\eta_{\text{G}}^{\lambda}, \tag{19}$$

where $\eta_{\text{M}}^{\lambda}$ and η_{G}^{λ} denote the efficiency of MG1 and MG2, λ is used to describe the operation state of the two electric machines, and is defined as:

$$\lambda = \begin{cases} 1, & \text{charging}, \\ -1, & \text{discharging}. \end{cases} \tag{20}$$

3 Hybrid control system modeling of HEV

There are different dynamic equations when the locking mechanism is engaged or disengaged. The switches between different modes are driven by events, and these events may rely on the continuous time-driven (continuous time, discrete-time, or mixed) states in each operation mode given by the differential or difference equations. When the continuous variables hit the predefined threshold, the continuous and discrete dynamics interact [24]. Aiming at the system that contains both time-driven continuous dynamics and event-driven discrete dynamics, various hybrid modeling methods are adopted to describe the hybrid systems [25,26].

In ref. [27], a hybrid control scheme, composing three distinct levels, is proposed to model the hybrid system, as shown in Figure 3. The plant is a continuous variable dynamic system (CVDS) described by differential equations, while the controller is viewed as a discrete event dynamic system (DEDS). The interface is designed to realize communication between CVDS and DEDS. The generator can generate symbols for the discrete events of the controller when the state variable moves between different regions, while the actuator generates the control input of the plant according to the controller symbols. When combined with the interface, the plant also becomes a DEDS. A discrete hybrid automaton control scheme, similar to this hybrid system framework, was presented in ref. [28], where the controller was described by a finite state machine (FSM), and the actuator was replaced by a mode selector to decide the mode in the plant level.

In the study, the model structure of the hybrid control system for the proposed HEV is inspired by the previous two kinds of hybrid system frameworks. The designed control structure is shown in Figure 4.

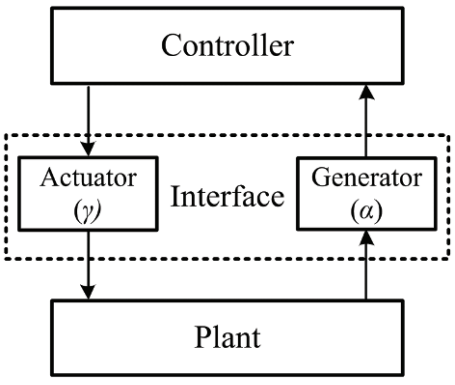

Figure 3 Hybrid control scheme.

A hybrid automaton is a formal model for the hybrid system by embedding the continuous differential equations into corresponding discrete states. The mathematical model of the hybrid control system is described by the following nine-tuple [29]:

$$H = (X_D, \Sigma, \delta; X_C, Y, U, f; \alpha, \beta). \tag{21}$$

(1) The supervisory controller is a DEDS described by (X_D, Σ, δ), and is driven by discrete events Σ_E. Σ_E: $\Sigma_S \cup \Sigma_U$ is the set of system finite discrete events, which consists of the event set Σ_S decided by the continuous variables of the plant (such as battery SOC and vehicle speed) and the event set Σ_U decided by the external disturbances (acceleration and brake pedal). Σ: $\Sigma_E \cup \Sigma_C$ is the set of the system events. Σ_C is the set of control decision events, such as the vehicle key on and off action. X_D= {m_{A}, m_{B}, m_{C}, m_{A1}, m_{A2}, m_{A3}, m_{A4} (m_{B1}), m_{B2}, m_{B3}, m_{C1}, m_{C2}} denotes the set of discrete states, and corresponds to the available modes as classified in Table 1. m_{A}, m_{B} and m_{C} are implicit and applied for better decision of the HEV finial operation mode. δ: $\Sigma \times X_D \rightarrow \Sigma$ is the transition function to control the discrete state transitions in the DEDS.

(2) As for the description of the plant, X_C is a finite set of continuous variables x: X_C={x: x=[ω_{E}, ω_{out}, v, SOC]$^{\text{T}}$} $\subseteq \boldsymbol{R}^4$. The evolution of powertrain states is described by the vector fields f: $X_C \times U_{\text{D}} \rightarrow X_C$. Since the power coupling device has different dynamics according to the states of the locking mechanism, different vector fields f_1 and f_2 are applied when the locking mechanism is disengaged or engaged. U: U= U_D $\cup$ U_E is the control space. U_D is a finite set of internal control variables u_d: U_D={u_d: u_d =[T_{E}, T_{M}, T_{G}, T_{Brk}, $Enable_{\text{E}}$, $Enable_{\text{L}}$]$^{\text{T}}$} $\subseteq \boldsymbol{R}^4 \times \{0,1\}^2$. $Enable_{\text{E}}$ =1 indicates that the engine is on, while $Enable_{\text{E}}$ =0 indicates that the engine is off. $Enable_{\text{L}}$=1 means that the locking mechanism is engaged; $Enable_{\text{L}}$=0 disengaged. U_E is a finite set of measurable external disturbances u_e: U_E={u_e: u_e=[T_{req}, v]$^{\text{T}}$}$\subseteq \boldsymbol{R}^2$.

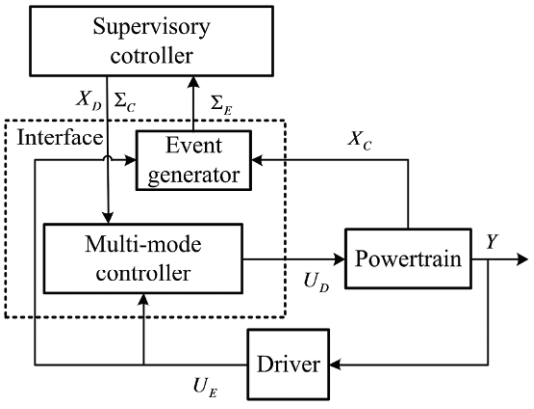

Figure 4 Hybrid control structure of the power split HEV.

T_{req} is the required torque at the wheels. For the simulation study, the values of accelerator and brake pedal are converted to the relevant torque requirements T_{req} obtained from a driver model with PI simulator. Y is the finite set of output variables y: $Y=\{y: y=[\omega_{\text{E}}, v, \text{SOC}, \dot{m}_f]^{\text{T}}\} \subseteq \boldsymbol{R}^4$, where $\dot{m}_f$ is the fuel consumption rate.

(3) (α, γ) depicts the role of the interface, which realize the connection and conversion between CVDS and DEDS. α: $X_C \cup U_E \rightarrow \Sigma_E$ maps the states space and measurable external disturbances to the discrete events Σ_E. γ: $X_D \cup U_E \cup \Sigma_C \rightarrow U_D$ is the map function representing the conversion from the set of discrete states, external measurable disturbances and control decision events to the control space. The map function γ is applied to decide the control vector u_d in the study. The optimal strategy to obtain the desired control values is applied in the multi-mode controller.

3.1 Interface

3.1.1 Event generator

With the variation of the state and disturbance inputs, HEV operates in different modes to maintain charging sustainability of the battery and optimize fuel economy. The transition of different states is decided by the combination of various events, which are generated in the interface level by the event generator. The definition of events is defined as:

$$\alpha=\begin{cases} q_1, & T_{\text{req}}>0, \\ q_2, & T_{\text{req}}=0, \\ q_3, & \text{SOC}>\text{SOC}_{lo}, \\ q_4, & v>v_{thresh}, \\ q_5, & T_{\text{req}}>T_{\text{Mlim}}, \\ q_6, & \omega_{\text{E}}>\omega_{\text{idle}}, \\ q_7, & \text{SOC}>\text{SOC}_{hi}, \\ q_8, & v>v_{reghi}, \\ q_9, & t>t_{\min}, \\ q_{10}, & \text{SOC}>\text{SOC}_{hichg}, \end{cases} \tag{22}$$

where q_i (i=1,2,…,10) denotes the events generated according to powertrain state variables and disturbance inputs. SOC_{lo} and SOC_{hi} are the lower limit and upper limit of the battery SOC, respectively. v_{thresh} is the vehicle speed used to decide whether the HEV should operate in electric driving mode. T_{Mlim} is the torque limit of MG2 which is used to judge whether the HEV should operate in compound electric driving mode. ω_{idle} is the engine idling speed. v_{reghi} is the speed limit to ensure that regenerative braking is disabled when vehicle speed is high. SOC_{hichg} is defined as the upper limit for state m_{B3}. To avoid frequent on/off operations of the engine, a minimum time interval $t_{\min}$ is defined.

3.1.2 Multi-mode controller

Based on the driver torque requirement and the selected discrete state from the supervisory controller, the multi-mode controller outputs the optimal control vector. For different states, the torque of the engine, MG1 and MG2 should be distributed optimally to fully improve the fuel economy, as well as to meet the requirements of SOC balance and physical constraints of the components. The torque distribution problems are mainly dealt with in three states: MG1 and MG2 compound driving, hybrid driving and charging while standstill. For the other driving modes, the torque can be ultimately determined according to the required driving torque. While the power split HEV is in braking mode, taking braking safety as the precondition, the friction braking torque and regenerative braking torque of MG2 are distributed to regenerate braking energy as much as possible.

By assuming that the inertia of the gear sets, engine, MG1 and MG2 are zero, the torque distribution can be calculated based on the static torque equilibrium model. This is reasonable [19]. Since there are two DoFs for power split vehicles, the optimal engine torque and speed are usually calculated firstly, and a PI controller is then designed to track the desired engine speed by controlling MG1 torque [15].

(1) MG1 and MG2 compound driving

In this state, both MG1 and MG2 are used to drive the vehicle. To improve fuel economy, the minimization of the electrical power loss should be maintained. Therefore, the optimization problem is formulated as:

$$\begin{aligned} &\min_{T_{\text{M}}} J=\int_{t_0}^{t_f} P_{\text{ele,loss}}\left(T_{\text{M}}(t),t\right)\text{d}t, \\ &\text{s.t. } \omega_{\text{M,min}}\leqslant\omega_{\text{M}}\leqslant\omega_{\text{M,max}},\ T_{\text{M,min}}\leqslant T_{\text{M}}\leqslant T_{\text{M,max}}, \\ &\qquad \omega_{\text{G,min}}\leqslant\omega_{\text{G}}\leqslant\omega_{\text{G,max}},\ T_{\text{G,min}}\leqslant T_{\text{G}}\leqslant T_{\text{G,max}}, \end{aligned} \tag{23}$$

where $\omega_{\text{M,max}}$ and $\omega_{\text{M,min}}$ are the maximum and minimum speed of MG2, while $\omega_{\text{G,max}}$ and $\omega_{\text{G,min}}$ are speed boundaries of MG1. $T_{\text{M,max}}$, $T_{\text{M,min}}$, $T_{\text{G,max}}$ and $T_{\text{G,min}}$ are the corresponding torque boundaries of MG2 and MG1. The battery is assumed to be designed with enough capacity to supply the motor and generator. The electrical power loss is

$$P_{\text{ele,loss}}=T_{\text{M}}\omega_{\text{M}}\left(\eta_{\text{M}}^{\lambda}-1\right)+T_{\text{G}}\omega_{\text{G}}\left(\eta_{\text{G}}^{\lambda}-1\right). \tag{24}$$

When the optimal MG2 torque T_{Mref} is calculated, the reference torque of MG1 is given by

$$T_{\text{G}}=-\frac{T_{\text{req}}/i_{\text{d}}-(1+K_2)T_{\text{Mref}}}{K_1}. \tag{25}$$

(2) Charging while standstill

MG1 is driven by engine to charge the battery. Constant operation point of the engine is selected. According to steady state torque relations, the required static torque of

MG1 is calculated from the engine reference torque T_{Eref}

$$T_{\text{Gstat}} = -\frac{T_{\text{Eref}}}{1+K_1}. \tag{26}$$

(3) Hybrid driving

The engine, MG1 and MG2 coordinate in this mode to drive the HEV. An alternative method to optimize the power flow is based on PMP [16,30]. The optimization problem is expressed as:

$$\begin{aligned}
&\min_{T_{\text{E}},\omega_{\text{E}}} J = \int_{t_0}^{t_f} \dot{m}_f\left(u(t),t\right)\mathrm{d}t,\\
&s.t.\ \dot{\text{SOC}} = f\left(x(t),u(t),t\right),\\
&\omega_{\text{E,min}} \leqslant \omega_{\text{E}} \leqslant \omega_{\text{E,max}},\ T_{\text{E,min}} \leqslant T_{\text{E}} \leqslant T_{\text{E,max}},\\
&\omega_{\text{M,min}} \leqslant \omega_{\text{M}} \leqslant \omega_{\text{M,max}},\ T_{\text{M,min}} \leqslant T_{\text{M}} \leqslant T_{\text{M,max}},\\
&\omega_{\text{G,min}} \leqslant \omega_{\text{G}} \leqslant \omega_{\text{G,max}},\ T_{\text{G,min}} \leqslant T_{\text{G}} \leqslant T_{\text{G,max}},
\end{aligned} \tag{27}$$

where x is the state variable of the system, i.e., the battery SOC, u is the engine operation point (T_{E}, ω_{E}). $\omega_{\text{E,min}}$ and $\omega_{\text{E,max}}$ are the engine minimum and maximum speed, while $T_{\text{E,min}}$ and $T_{\text{E,max}}$ are the lower and upper limit of engine torque, respectively. According to PMP, the Hamiltonian is defined as:

$$H = \dot{m}_f(t) + p(t) f\left(x(t),u(t),t\right), \tag{28}$$

where p is the co-state. The variation of the co-state can be depicted as:

$$\dot{p} = -\frac{\partial H}{\partial x} = -\frac{\partial f}{\partial x}. \tag{29}$$

The optimal control variable T_{E} and ω_{E} derived from PMP also ensure the following conditions to be satisfied, which is necessary but not sufficient for the global optimization

$$H\left(x,u^*,p,t\right) = \min H\left(x,u,p,t\right). \tag{30}$$

It is worthy to mention that, in order to maintain charge sustainability, the final SOC of the battery at the end of the driving cycle should be equal to that of the initial value. However, since it is difficult to achieve this, the final SOC of the battery is usually controlled within a certain region [31].

After the optimal engine torque and speed are calculated in the multi-mode controller, the required static torque of MG1 can also be derived according to eq. (26). Reference torque of MG2 is calculated according to the engine reference torque and T_{req}

$$T_{\text{Mref}} = \frac{T_{\text{req}}}{i_{\text{d}}\left(1+K_2\right)} - \frac{K_1 T_{\text{Eref}}}{\left(1+K_1\right)\left(1+K_2\right)}. \tag{31}$$

In the forward simulation, the engine speed cannot be directly controlled. A PI controller is designed to track the engine reference speed by controlling the torque of MG1 [15]. The control scheme of MG1 is shown in Figure 5. The reference torque T_{Gref} of MG1 is obtained as the summation of the static torque T_{Gstat} and the dynamic compensation torque ΔT_{G} generated by PI module .

3.2 Supervisory controller

The FSM is used to depict the event-driven dynamics of the supervisory controller and the transitions between different discrete states, as shown in Figure 6. Firstly, three main states of the vehicle, i.e., driving, standstill and braking, are decided by the events obtained from required torque T_{req}. In each of the three states, the HEV final operation mode will be further decided.

The conditions of transitions between different states are evaluated at each sample time. When the vehicle velocity is below a certain value v_{thresh} and the battery SOC is higher than the lower limit SOC_{lo}, the vehicle is driven by MG2, and MG1 will provide assistive torque if the required torque of MG2 is larger than its torque limit T_{Mlim}. Otherwise, the engine is activated. During braking, to guarantee braking safety, the regenerative braking is disabled if the vehicle velocity is larger than v_{reghi}. When the battery SOC is higher than SOC_{hi}, regenerative braking is also disabled to prevent the battery from over charging. It is worth noting that the mechanical braking system will provide assistive friction torque if MG2 cannot supply enough regenerative torque. Such compound braking is included in the regenerative

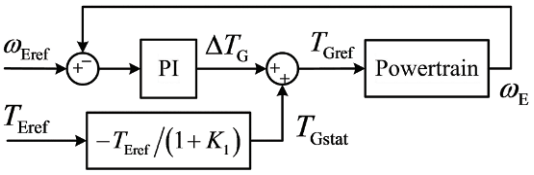

Figure 5 Block diagram of PI controller for MG1.

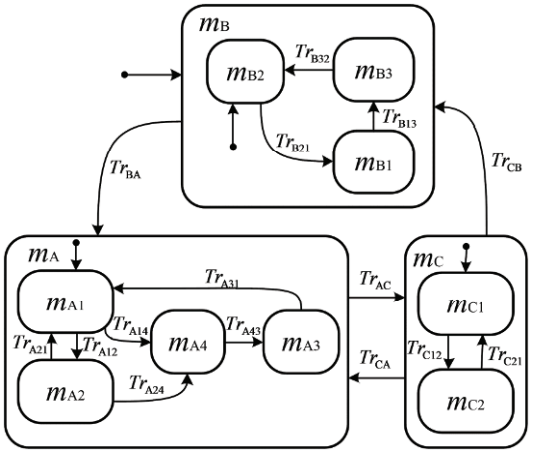

Figure 6 Event driven supervisory control structure.

braking. When the vehicle is at standstill, battery charging by the engine is allowed if the battery SOC is below SOC_{hichg}. More specifically, the transition conditions are listed in Table 2.

4 Energy optimization management

In Section 3, when, based on PMP only in hybrid driving mode, optimal method is implemented, there are limitations to fully improve the fuel economy. Since the locking mechanism is engaged only when compound pure electric driving is required, the model-based optimal control strategy can be applicable for the operation modes represented by the same control-oriented model.

In this section, the nonlinear model predictive control (NMPC) strategy is used to optimize the power flow, which is adopted in the multi-mode switch controller. The operation states of the HEV are reclassified, and the event-driven dynamics in the supervisory controller is shown in Figure 7. The vehicle driving mode and standstill mode are integrated and denoted by m_{A}. The compound pure electric driving mode is represented by m_{A2}, while other modes of driving and standstill as shown in Table 1 can be unified as m_{A1}. The definition of braking is the same as that described in Section 3.2. The transition conditions are specified and listed in Table 3.

When the power split HEV operates in m_{A1}, the NMPC strategy is adopted. The MPC algorithm solves the optimal problem in the prediction horizon and obtains a sequence of optimal control inputs. Only the first control input is applied to the plant. The vehicle speed and/or torque demands can be predicted when performing MPC strategy [19,32]. DP algorithm is capable of finding the global optimization solutions for a priori knowledge [33]. Consequently, DP can be implemented over a receding finite horizon to solve the nonlinear and constrained optimization problem of MPC.

Table 2 Transition conditions between different states

Transition	Condition	Transition	Condition
Tr_{AC}	$\sim(q_1 \vee q_2)$	Tr_{A31}	$\sim q_4 \wedge q_3 \wedge q_9$
Tr_{CA}	q_1	Tr_{A43}	q_6
Tr_{BA}	q_1	Tr_{B13}	q_6
Tr_{CB}	q_2	Tr_{B21}	$\sim q_6 \wedge \sim q_{10}$
Tr_{A12}	$q_5 \wedge q_3 \wedge \sim q_4$	Tr_{B32}	q_{10}
Tr_{A14}	$(\sim q_3 \vee q_4) \wedge q_9$	Tr_{C12}	$q_7 \vee q_8$
Tr_{A21}	$\sim q_5 \wedge q_3 \wedge \sim q_4$	Tr_{C21}	$\sim q_7 \wedge \sim q_8$
Tr_{A24}	$(\sim q_3 \vee q_4) \wedge q_9$	–	–

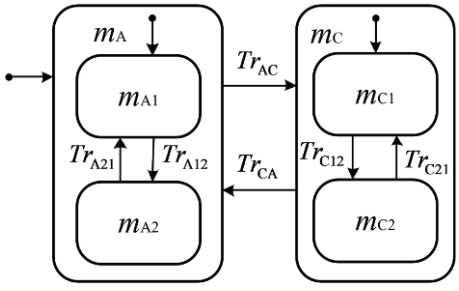

Figure 7 Event driven dynamics with optimization management.

Table 3 Transition conditions between different states

Transition	Condition	Transition	Condition
Tr_{AC}	$\sim(q_1 \vee q_2)$	Tr_{A21}	$(\sim q_3 \vee q_4) \wedge q_9$
Tr_{CA}	$q_1 \vee q_2$	Tr_{C12}	$q_7 \vee q_8$
Tr_{A12}	$q_5 \wedge q_3 \wedge \sim q_4 \wedge q_9$	Tr_{C21}	$\sim q_7 \wedge \sim q_8$

The time domain is divided into finite stages to implement NMPC. The optimization problem must attain two objectives. The first objective is to get the maximum fuel economy, while the second one is to maintain charge sustaining [34]. Assuming that the prediction horizon is *Np*, the cost-to-go function of the NMPC optimal problem is described as:

$$\begin{aligned} J &= \sum_{k=0}^{Np-1} L\big(x(k),u(k)\big) \\ &= \sum_{k=0}^{Np-1}\Big[r_f \dot{m}_f(k)\Delta t + r_{SOC}\big(\mathrm{SOC}(k)-\mathrm{SOC}_{\mathrm{ref}}\big)^2\Big], \end{aligned} \tag{32}$$

where L is the cost at the stage k. $\mathrm{SOC}_{\mathrm{ref}}$ is the reference battery SOC value. Δt is the discrete time step. r_f and r_{SOC} are the weighting factors. The final battery SOC is often set equal to the initial SOC to guarantee charge sustaining when performing DP [15,34]. It is unreasonable for NMPC to ensure this condition in the finite horizon. Therefore, the deviation of the actual SOC to the reference value is introduced as constraint in the cost-to-go function.

The optimal solution Π^* is programmed in the prediction horizon. The battery SOC is the dynamic state, and the engine torque and speed are chosen as the control variables. According to Bellman principle, the optimal problem is described by

$$\begin{aligned} &\Pi^* = \arg\min J_0^*\big(x(0)\big), \\ &J_k^*\big(x(k)\big) = \min_{u(k)}\Big[L\Big(\big(x(k),u(k)\big)\Big) + J_{k+1}^*\big(x(k+1)\big)\Big], \\ &J_{Np}^*\big(x(Np)\big) = 0. \end{aligned} \tag{33}$$

This optimal process should also be conducted on the basis of the HEV physical constraints as denoted by eq. (27). The SOC is divided into finite steps from SOC_{lo} to SOC_{hi} at each stage. Therefore, the SOC constraints are automatically satisfied according to this discretization, and the battery dynamics is

$$\mathrm{SOC}(k+1) = \mathrm{SOC}(k) - \frac{V_{\mathrm{oc}} - \sqrt{V_{\mathrm{oc}}^2 - 4P_{\mathrm{bat}}R_{\mathrm{int}}}}{2Q_{\mathrm{bat}}R_{\mathrm{int}}}\Delta t. \tag{34}$$

To further ease the computation burden, constant efficiencies of the components are used. The control variables, engine torque and speed, are discretized according to the engine optimal operation line (OOL), as shown in Figure 8. OOL can be calculated through the following steps: (1) The engine power is equally divided into finite steps from 0 to the maximum engine power P_{Emax}; (2) for each divided point of the engine power, the fuel consumption rates of a series of engine operation points (T_{E}, ω_{E}) are calculated, and the operation point corresponding to the minimum fuel consumption is selected; (3) the operations points for all the divided engine power points are plotted and connected in the engine map. In this way, the grids of control variables are greatly reduced by searching along the OOL instead of the whole engine map.

5 Simulation and analysis

To demonstrate the performance of the developed power split system and control strategy, comparative simulations are conducted for the New European driving cycle (NEDC), which consists of four repeated urban driving cycles and one extra-urban driving cycle, and Urban Dynamometer driving schedule (UDDS), as shown in Figure 9. The FSM is implemented in the MATLAB/Stateflow toolbox. The specifications of the power split HEV are given in Table 4, and the control parameters are listed in Table 5.

Responses of the power split HEV are shown in Figures 10 and 11 for NEDC and UDDS scenarios, respectively. The control strategy proposed in Section 3 is named as strategy A, where the strategy based on PMP is designed to split power for the hybrid driving mode. The other strategy introduced in Section 4 is denoted by strategy B. Battery SOC plots, as shown in Figures 10(a) and 11(a), indicate that the charging sustainability is well guaranteed when applying the proposed two control strategies. The SOC curve with strategy B shows a smoother tendency than that of strategy A. Since the ring gear of PG2 is fixed, the direction of MG2 speed is the same as the speed direction at the input side of the final drive. The speed of MG2 is also proportional to the wheel speed. Consequently, when the torque

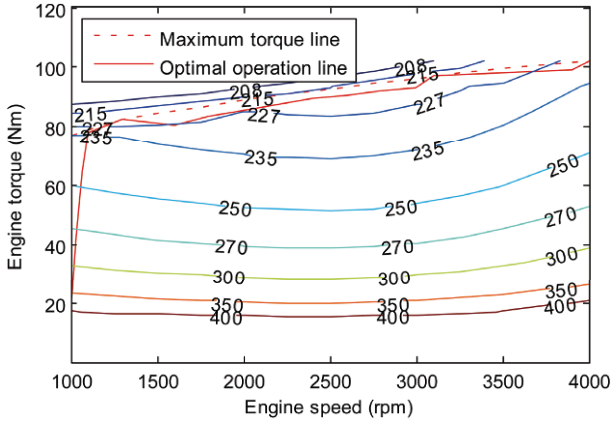

Figure 8 (Color online) Engine fuel consumption map.

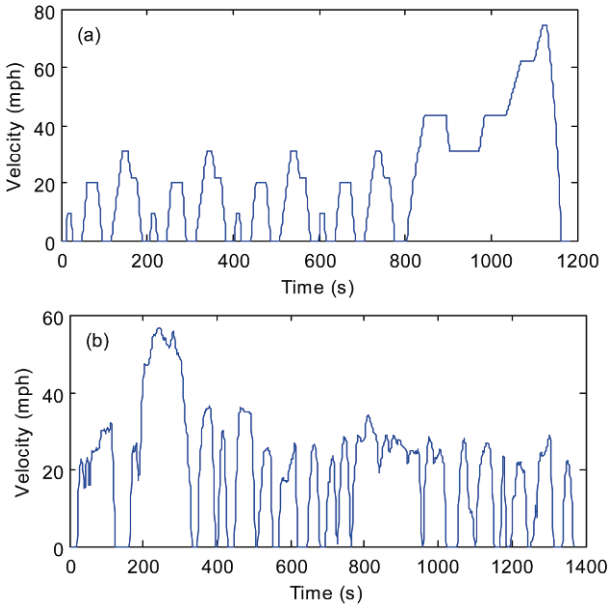

Figure 9 (Color online) Driving cycles. (a) NEDC; (b) UDDS.

Table 4 Specifications of power split HEV

Parameter	Value
Wheel radius R_w	0.287 m
Coefficient of rolling resistance f	0.008
Air density ρ_{air}	1.23 $\mathrm{m^3/kg}$
Air drag coefficient C_{d}	0.3
Vehicle frontal area A_f	1.746 $\mathrm{m^2}$
Ratio of the final drive i_{d}	3.93
Characteristic parameter of PG1 K_1	2.11
Characteristic parameter of PG1 K_2	2.11
Engine maximum power $P_{\mathrm{E\_max}}$	54 kW
Engine maximum speed $\omega_{\mathrm{E\_max}}$	700 rpm
Inertia of engine I_{E}	0.072 kg $\mathrm{m^2}$
MG1 maximum power $P_{\mathrm{E\_max}}$	15 kW
MG1 maximum speed $\omega_{\mathrm{G\_max}}$	8000 rpm
Inertia of MG1 I_{G}	0.022 kg $\mathrm{m^2}$
MG2 maximum power $P_{\mathrm{E\_max}}$	30 kW
MG2 maximum speed $\omega_{\mathrm{M\_max}}$	15000 rpm
Inertia of MG2 I_{M}	0.030 kg $\mathrm{m^2}$

Table 5 Specifications of controller

Parameter	Value
Engine speed range region [ω_{low} ω_{ip}] (rpm)	[1000 3500]
SOC range [$\mathrm{SOC_{lo}}$ $\mathrm{SOC_{hi}}$]	[0.4 0.7]
SOC_{hichg}	0.55
$\mathrm{SOC_{ini}}$	0.55
v_{thresh} (km/h)	32
V_{reghi} (km/h)	80
T_{Mlim} (Nm)	180
Np	10

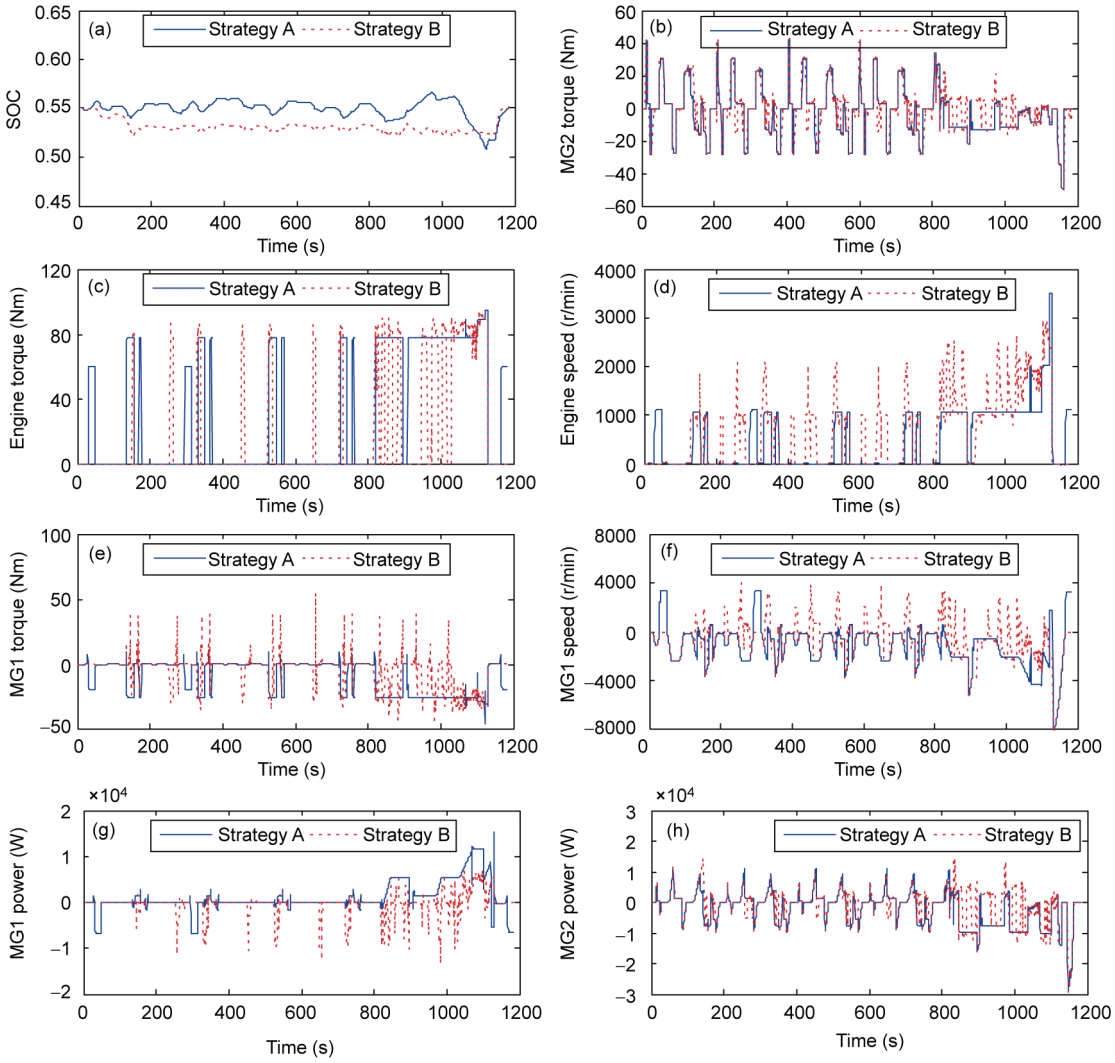

Figure 10 (Color online) Simulation results for NEDC. (a) Battery SOC; (b) torque of MG2; (c) engine torque; (d) engine speed; (e) torque of MG1; (f) speed of MG1; (g) power of MG1; (h) power of MG2.

of MG2 is negative, MG2 regenerates the braking energy.

From the engine torque responses in Figures 10(c) and 11(c), it can be observed that the rest time of engine with strategy A is longer than that with strategy B. However, the engine shows more frequent start and stop when NMPC is applied for the extra-urban driving cycle of NEDC. This may lead to more energy consumption when strategy B is practically used regarding the engine transient characteristics. Besides, frequent engine start and stop will cause longitudinal shocks. The optimization strategy needs to be improved to avoid frequent start and stop of the engine. For UDDS cycle, the engine shows more frequent on/off states than those for NEDC. It is because that the UDDS cycle, which is for the dynamometer test, has more fluctuations with accelerations and decelerations. The HEV is frequently switched to braking mode, where the engine is shut off. Figures 10(d) and 11(d) illustrate the engine speed for the two driving cycles. The average speed of the engine is higher when strategy B is used. This ensures the engine to operate in the high efficiency region. By comparing the figures of engine torque and speed, it can be seen that the engine speed is regulated to be zero or idling when the engine doesn't start. In some cases, the engine is at the idling speed instead of zero if it is shut off. The engine start strategy should be further improved in following studies.

The torque and speed of MG1 are given in Figure 10(e) and 10(f) for NEDC cycle, while Figure 10(g) and 10(h) describe the power of MG1 and MG2. Similar descriptions are applied to Figure 11(e)–(h) for UDDS cycle. It is obvious that the rated power of MG1 and MG2 meet the driving requirements. In most time regions, MG1 generates electricity. Nevertheless, the contrary is the case when the vehicle speed is high. In this case, MG1 is used to drive the vehicle while MG2 generates electricity. The reason is that the speed of MG1 is closely related to the engine speed and vehicle speed, as shown in eq. (5). If the engine speed is

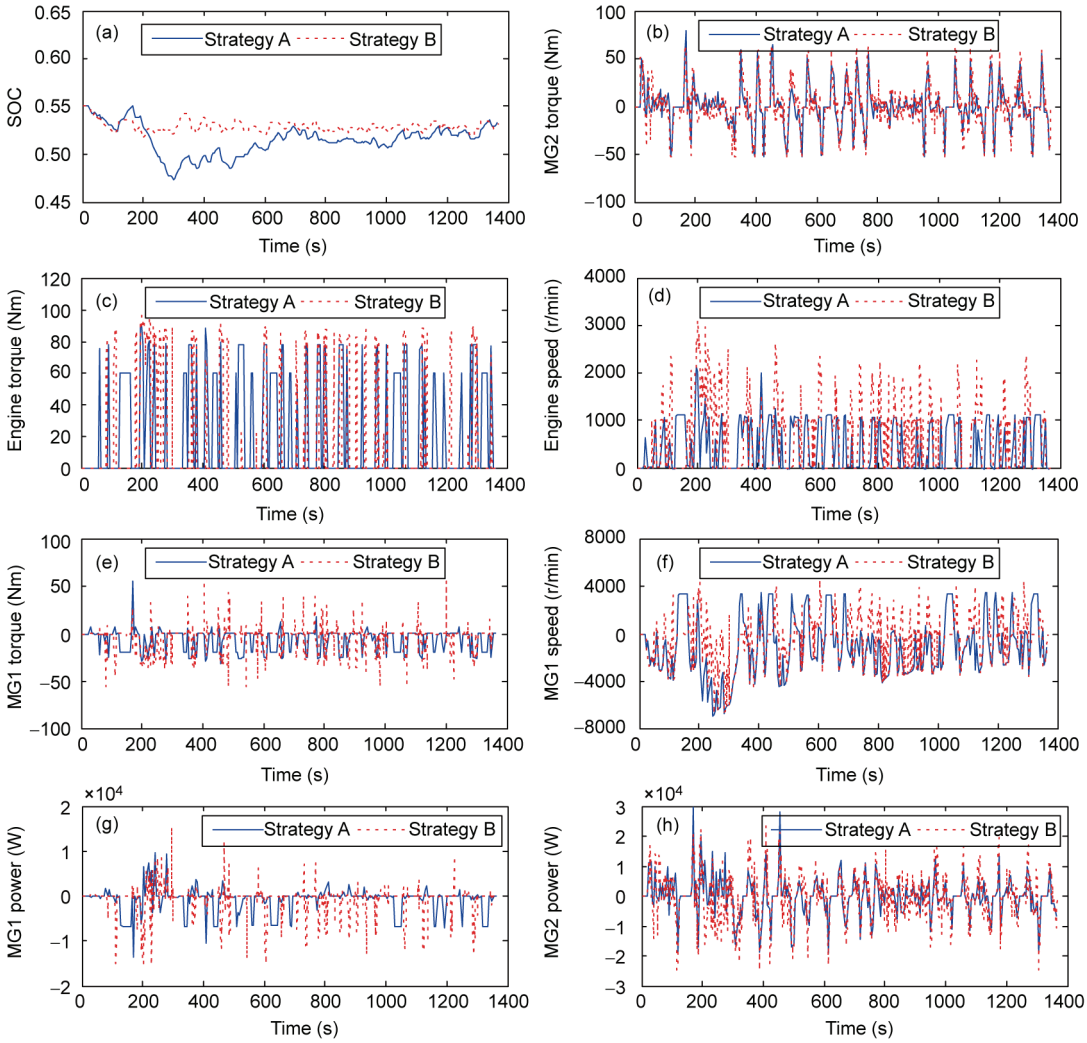

Figure 11 (Color online) Simulation results for UDDS. (a) Battery SOC; (b) torque of MG2; (c) engine torque; (d) engine speed; (e) torque of MG1; (f) speed of MG1; (g) power of MG1; (h) power of MG2.

low and the vehicle speed is high, the speed of MG1 is opposite to that of the engine. Consequently, the power of MG1 is positive and MG1 consumes electrical energy. According to eq. (31), the torque of MG2 will be negative if the engine torque is large, and MG2 will regenerate energy. Figures 10(g) and 11(g) also indicate that the power of MG1 used to regulate the engine speed is nearly zero. It validates the feasibility to synthesize the operation modes.

To better describe the engine working conditions, engine operation points for NEDC and UDDS cycles are illustrated in the engine map, as shown in Figure 12. With PMP and NMPC optimal methods, most of the engine points are located in the high efficiency regions. Since the engine speed and torque are searched along the engine OOL when NMPC is being implemented in strategy B, most of the engine operating points distribute along this optimal line.

In Table 6, comparisons between the MPG and battery SOC at the end of the driving cycle for different control strategies are made. It is observed that the HEV fuel economy is improved when strategy B is applied, especially for the NEDC cycle, where the MPG is increased by 8.8%. However, the improvement of fuel economy with NMPC for the UDDS cycle is not so apparent in comparison with the case for NEDC. One possible reason for lower MPG with strategy A is that constant engine operation point (1100 rpm-60 Nm) is adopted to charge the battery for the charging while standstill mode. The brake specific fuel consumption (BSFC) at this point is about 238 g/kW h. This operation point, chosen as a compromise to reduce fuel consumption and maintain the battery charge sustainability, is overlapped in the engine map and is not in the high efficiency region, thereby, resulting in more fuel consumption.

6 Conclusions

The dynamic model of a power split device is established on the basis of level analogy for the HEV forward simulation.

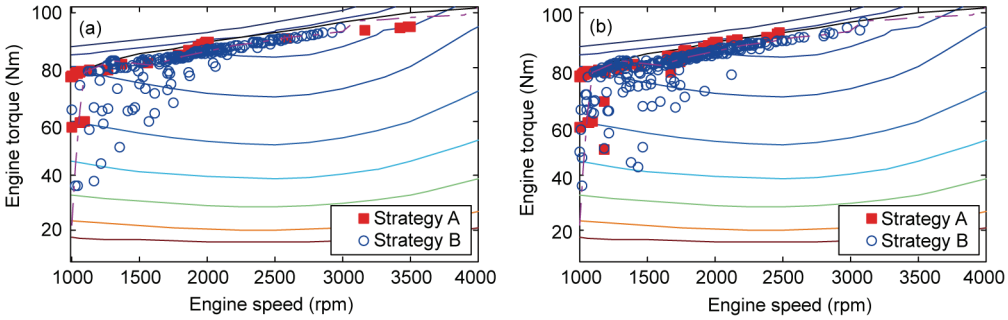

Figure 12 (Color online) Engine operation points. (a) Engine operation points for NEDC; (b) engine operation points for UDDS.

Table 6 Fuel consumption in MPG of HEV for different cases

Cycle	Strategy A		Strategy B	
	MPG	Final SOC	MPG	Final SOC
NEDC	69.4	0.551	75.5	0.549
UDDS	86.1	0.534	89.7	0.531

By analyzing the operation principle of the HEV, feasible operation modes are selected, and the operation process is found to be featured by the interactions between discrete dynamics and continuous dynamics. Consequently, the control structure is constructed on the basis of hybrid automaton control theory. In the controller, the HEV mode transitions are described by FSM as discrete dynamics, and are driven by events generated from the event generator of the interface. The multi-mode switch controller is designed to calculate the plant control inputs.

Feasible operation modes are listed and selected according to the predefined rules. The optimal control strategy based on PMP is adopted to split the power among the engine, MG1 and MG2 for the hybrid driving mode. To further improve the HEV fuel economy, the operation modes are synthesized. With the minimization of fuel consumption and the sustainability of the battery as two targets, DP is implemented in the prediction horizon to solve the optimization problem in a NMPC framework.

Comparative simulation results demonstrate that the hybrid control structure of the HEV is feasible for the application of various optimal control strategies. The proposed energy management strategies show good performance in splitting the HEV power and maintain the battery charge sustainability. When the operation modes are synthesized and in conjunction with NMPC, the MPG is improved by 8.8% for NEDC cycle. However, the frequent engine start and stop caused by the NMPC optimal strategy still needs to be addressed in our following studies. The proposed dynamic model and control methods provide bases for the design of optimal energy management.

This work was supported by the Priority Academic Program Development of Jiangsu Higher Education Institutions (PAPD), the National Natural Science Foundation of China (Grant Nos. 51475213 & 51305167), and the Scientific Research Innovation Projects of Jiangsu Province (Grant No. KYLX_1022).

1 Huang K D, Tzeng S C. A new parallel-type hybrid electric-vehicle. Appl Energy, 2004, 79: 51–64
2 Bayindir K Ç, Gözüküçük M A, Teke A. A comprehensive overview of hybrid electric vehicle: Powertrain configurations, powertrain control techniques and electronic control units. Energ Convers Manag, 2011, 52: 1305–1313
3 Zhang X, Peng H, Sun J, et al. Automated modeling and mode screening for exhaustive search of double-planetary-gear power split hybrid powertrains. In: Proceedings of ASME 2014 Dynamic Systems and Control Conference. San Antonio, Texas: IEEE, 2014
4 Burress T A, Cmpell S L, Coomer C L, et al. Evaluation of 2010 Toyota Prius hybrid synergy drive system. Technical Report. Washington: Oak Ridge National Laboratory, 2011. ORNL/TM-2010/253
5 Miller J M. Hybrid electric vehicle propulsion system architectures of the e-CVT type. IEEE T Power Electron, 2006, 21: 756–767
6 Wishart J D, Zhou Y, Dong Z. Review, modelling and simulation of two-mode hybrid vehicle architecture. In: Peoceedings of 9th International Conference on Advanced Vehicle and Tire Technologies (AVTT). Las Vegas: ASME, 2007
7 Zhang X, Li C T, Kum D, et al. Prius$^+$ and Volt$^-$: Configuration analysis of power-split hybrid vehicles with a single planetary gear. IEEE T Veh Tech, 2012, 61: 3544–3552
8 Chen L, Zhu F, Zhang M, et al. Design and analysis of an electrical variable transmission for a series–parallel hybrid electric vehicle. IEEE T Veh Tech, 2011, 60: 2354–2363
9 Zhuang W, Zhang X, Ding Y, et al. Comparison of multi-mode hybrid powertrains with multiple planetary gears. Appl Energy, 2016, 178: 624–632
10 Taghavipour A, Azad N L, McPhee J. Design and evaluation of a predictive powertrain control system for a plug-in hybrid electric vehicle to improve the fuel economy and the emissions. Proc IMechE, Part D-J Automob Eng, 2014, 229: 624–640
11 Panday A, Bansal H O. A review of optimal energy management strategies for hybrid electric vehicle. Int J Veh Technol, 2014, 2014: 160510
12 Mashadi B, Emadi S A. Dual-mode power-split transmission for hybrid electric vehicles. IEEE T Veh Tech, 2010, 59: 3223–3232
13 Chen Z, Mi C C, Xiong R, et al. Energy management of a power-split plug-in hybrid electric vehicle based on genetic algorithm and quadratic programming. J Power Sources, 2014, 15: 416–426
14 Zhou M L, Lu D K, Li W M, et al. Optimized fuzzy logic control strategy for parallel hybrid electric vehicle based on genetic algorithm. Appl Mech Mater, 2013, 274: 345–349
15 Cipek M, Pavković D, Petrić J. A control-oriented simulation model of a power-split hybrid electric vehicle. Appl Energ, 2013, 101: 121–133
16 Kim N, Cha S W, Peng H. Optimal equivalent fuel consumption for hybrid electric vehicles. IEEE T Control Syst Tech, 2012, 20: 817–825
17 Kim N, Cha S, Peng H. Optimal control of hybrid electric vehicles based on Pontryagin's minimum principle. IEEE T Control Syst Tech, 2011, 19: 1279–1287

18 Skugor B, Deur J, Cipek M, et al. Design of a power-split hybrid electric vehicle control system utilizing a rule-based controller and an equivalent consumption minimization strategy. Proc Part D-J Automob Eng, 2014, 228: 631–648
19 Borhan H, Vahidi A, Phillips A M, et al. MPC-based energy management of a power-split hybrid electric vehicle. IEEE T Control Syst Tech, 2012, 20: 593–603
20 Yan F, Wang J, Huang K. Hybrid electric vehicle model predictive control torque-split strategy incorporating engine transient characteristics. IEEE T Veh Tech, 2012, 6: 2458–2467
21 Qin K J, Wang E H, Zhao H, et al. Development and experimental validation of a novel hybrid powertrain with dual planetary gear sets for transit bus applications. Sci China Tech Sci, 2015, 58: 2085–2096
22 Zhang R, Chen Y. Control of hybrid dynamical systems for electric vehicles. Proc Am Control Conf, 2001, 4: 2884–2889
23 Zhu Y, Chen Y, Wu Z, et al. Optimisation design of an energy management strategy for hybrid vehicles. Int J Altern Propul, 2006, 1: 47–62
24 Branicky M S, Borkar V S, Mitter S K. A unified framework for hybrid control: Model and optimal control theory. IEEE T Autom Control, 1998, 43: 31–45
25 Heemels W P, De Schutter B, Bemporad A. Equivalence of hybrid dynamical models. Automatica, 2001, 37: 1085–1091
26 Xue L, Liao M, Wei C, et al. Hybrid system and its modeling. Acta Simulata Syst Sin, 2004, 3: 003
27 Antsaklis P J, Stiver J A, Lemmon M. Hybrid system modeling and autonomous control systems. Hybrid Sys, 1993, 736: 366–392
28 Torrisi F D, Bemporad A. HYSDEL-A tool for generating computational hybrid models for analysis and synthesis problems. IEEE T Control Syst Tech, 2004, 12: 235–249
29 Wang S H. Research on multi-mode switching control of semi-active air suspension hybrid system. Dissertation for the Doctoral Degree. Zhenjiang: Jiangsu University, 2013
30 Xia C, Zhang C. Real-time optimization power-split strategy for hybrid electric vehicles. Sci China Tech Sci, 2016, 59: 814–824
31 HomChaudhuri B, Lin R, Pisu P. Hierarchical control strategies for energy management of connected hybrid electric vehicles in urban roads. Transp Res Part C-Emerg Tech, 2016, 62: 70–86
32 Sun C, Hu X, Moura S J, et al. Velocity predictors for predictive energy management in hybrid electric vehicles. IEEE T Control Syst Tech, 2015, 23: 1197–1204
33 Zhang L, Qi B, Zhang R, et al. Powertrain design and energy management of a novel coaxial series-parallel plug-in hybrid electric vehicle. Sci China Tech Sci, 2016, 59: 618–630
34 Pisu P, Rizzoni G. A comparative study of supervisory control strategies for hybrid electric vehicles. IEEE T Control Syst Tech, 2007, 15: 506–518